Paper

Control Strategies for Brushless Doubly Fed Reluctance Machines

Milutin G. Jovanović[1] and Robert E. Betz[2]
[1]School of Engineering, University of Northumbria at Newcastle
Newcastle upon Tyne NE1 8ST, UK
Fax : +44-191-2273684; e-mail : milutin.jovanovic@unn.ac.uk

[2]Department of Electrical and Computer Engineering
University of Newcastle, NSW 2308, Australia
Fax : +61-2-49216993; e-mail : reb@ecemail.newcastle.edu.au

Abstract— **Brushless doubly-fed machines (BDFMs) have been extensively researched over the last 15 years because they allow the use of a partially rated inverter in many variable speed applications. In its cage form the machine has substantial rotor losses and compromised efficiency. However, a reluctance version of the BDFM, the brushless doubly-fed reluctance machine (BDFRM), ideally has no rotor losses and therefore offers the potential for greater efficiency and much simpler control. To date a truly comprehensive and machine independent theoretical analysis of the BDFRM's optimal control properties has not been carried out. This paper will attempt to fill this void by considering the theoretical performance limitations of various control strategies for the machine, including maximum torque per inverter ampere, maximum torque per total ampere, maximum power factor of the two windings and associated trade-offs.**

Keywords— **brushless, reluctance machines, optimal control.**

I. Introduction

The advent of power electronics and microprocessors has largely contributed to the renewal of interests in the Brushless Doubly Fed Reluctance Machine (BDFRM) recently [1–8]. Owing to its slip power recovery operating nature, a feeding converter has to process at most half the machine's output power which means that significant capital cost savings can be made especially in larger drive systems regardless of the increased cost of the machine itself [3]. This is particularly the case if the required variable speed range is restricted, as the inverter size can be further reduced. However, special procedures have to be utilised for machine starting [5]. An additional advantage of the lower inverter rating is the better supply quality, as less harmonics are injected into the power grid.

These attributes make the BDFRM an ideal candidate for "niche" applications such as variable-speed constant-frequency (VSCF) hydro and wind power generation [2], as well as commercial and industrial heating, ventilation, and air conditioning (HVAC). Because of its ruggedness, enhanced reliability and lower maintenance afforded by the absence of brush gear, it is also a preferable solution for pump-type applications that have been traditionally served by the slip ring induction machine.

As illustrated in Fig. 1, the BDFRM has two stator windings of different pole numbers and a rotor similar to that of the synchronous reluctance machine (SYNCREL). Unlike a conventional machine, the rotor needs to have half the total number of stator poles in order to provide magnetic coupling between the windings, and therefore torque production [1, 3, 4]. Normally one winding, known as the primary or power winding, is connected to the mains supply (with fixed voltage and frequency), whereas the other is inverter fed, and is called the secondary winding or the control winding.

A closely related machine to the BDFRM, the Brushless Doubly Fed Induction Machine (BDFIM), uses a special rotor cage design composed of nested loops (Fig. 1). As with the BDFRM, the number of nests must be equal to the sum of the stator pole-pairs for the electromechanical energy conversion to occur in the machine. Clearly, the BDFRM with its cageless rotor structure should be more efficient, easier to model and thus simpler to control as compared to the BDFIM. The efficiency of the *inverter-fed* BDFRM, as compared to the inverter-fed BDFIM, has recently been experimentally verified [9]. This paper will consequently limit its discussion to the BDFRM.

The existing literature on the BDFRM control has focused on specific applications [2] or control aspects [4–6] but has not generally analysed the machine to determine its ***theoretical performance limitations***. The aim of this paper is to perform this kind of study. It will establish and closely examine the control set-point conditions for the following control objectives:

1. Maximum torque per secondary ampere.
2. Maximum torque per total primary and secondary winding amperes.
3. Unity power factor of the windings.

The performance analysis of the different control strategies undertaken in this paper can be used as a "figure of merit" against which the performance of real controllers can be measured.

In the following analysis it is assumed that the shaft

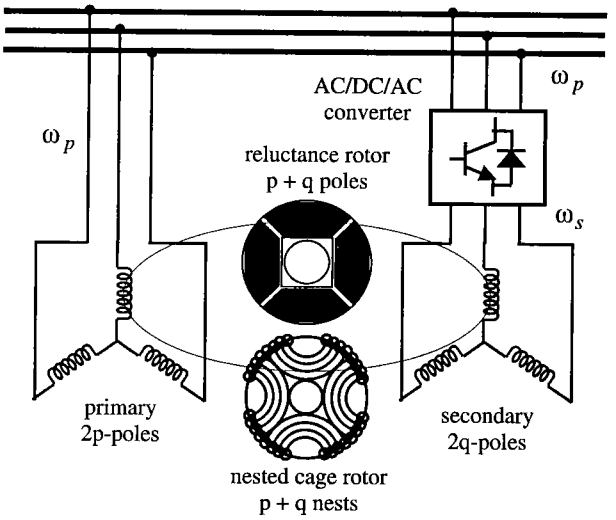

Fig. 1. A structural diagram of the BDFM with an axially-laminated and a cage rotor construction

position is available (via measurement). If required, sensorless control strategies can be devised for this machine [4], and the position transducer can be eliminated.

The development of the expressions used in this paper is very detailed and complicated. References [10, 11] are recommended for the interested reader.

II. Control Aspects

The subsequent analysis assumes an ideal machine without saturation. This simplification allows the derivation of mathematical expressions that form the basis for the development of vector control, and performance measures for "real" machines.

A. Maximum Torque Per Secondary Ampere

A desirable property for a BDFRM is to maximise the torque produced for a given inverter current rating – i.e. maximise the torque per secondary winding ampere (MTPSA). It can be shown that the machine torque, when the reference frame high permeance axis (d_p-axis) is aligned with the primary winding flux vector ($\omega = \omega_p$ in Fig. 2), can be expressed as [5, 7]:

$$T = \frac{3}{2} p_r \frac{L_{ps}}{L_p} \lambda_p i_{sq} = \frac{3}{2} p_r \frac{L_{ps}}{L_p} \lambda_p i_s \sin \alpha_s \qquad (1)$$

where $p_r \triangleq$ number of rotor poles, $L_p \triangleq$ primary winding inductance, $L_{ps} \triangleq$ primary to secondary mutual inductance, $\lambda_p \triangleq$ primary winding flux linkage (a constant), $i_{sq} \triangleq q$-axis secondary winding current and $\alpha_s \triangleq$controllable secondary current angle (Fig. 2). The definitions of the above three-phase inductances can be found in [8].

One should emphasise that (1) is the basic form that one would use for torque control [5]. This expression is identical to that for a standard wound rotor induction machine (WRIM) in a stator flux oriented reference frame. It is important to stress this as the BDFRM and the WRIM have essentially the same d-q model [1], and can share similar control schemes [4, 12] despite a fundamentally different principle of operation [3, 4].

We can immediately see from (1) that the torque-per-secondary-ampere (T/i_s) is a maximum if $\alpha_s = \pi/2$. It has been demonstrated in the previous work of the authors [8], that in this respect, the BDFRM can not compete favourably with the axially laminated SYNCREL, under the condition of the same copper losses and the same amount of active material in both the machines.[1] The reason for this is the quite peculiar torque producing mechanism of the BDFRM resulting in relatively weak magnetic coupling between the windings and modest L_{ps}/L_p values [3, 4]. This implies that a *larger* BDFRM is required, and a cost penalty on the machine side is to be paid relative to the similarly rated SYNCREL, or an equivalent cage induction machine. However, the *total system cost* of a BDFRM based drive can still be lower because of the much smaller inverter rating (this is particularly true in medium to large systems where the inverter cost is a significant component of the overall system cost).

It is opportune to now consider the *real* power rating of the inverter in a BDFRM system. This rating is obviously dictated by the proportion of the shaft power that is supplied by the secondary winding of the machine. This in turn can be shown to be related to the generalised slip of the machine[2] which is defined as:

$$s = -\frac{\omega_s}{\omega_p} \qquad (2)$$

where $\omega_p \triangleq$ the primary winding frequency, and $\omega_s \triangleq$ the secondary winding frequency.

It has been shown [10, 11] that the primary winding and secondary winding rotational powers are:[3]

$$P_{p_{\text{rot}}} = \frac{\omega_p}{p_r} T_e \qquad (3)$$

$$P_{s_{\text{rot}}} = \frac{\omega_s}{p_r} T_e \qquad (4)$$

where $p_r \triangleq$ the number of rotor poles and $T_e \triangleq$ the electromagnetic torque. The total rotational output is obviously $P_{\text{rot}} = P_{s_{\text{rot}}} + P_{p_{\text{rot}}} = \omega_{rm} T_e$ where $\omega_{rm} \triangleq$ the rotor mechanical angular velocity.[4]

Equation (4) can be arranged in terms of the machine

[1] The comparison with the axially laminated SYNCREL can be taken as an approximate comparison with the induction machine due to the performance similarity between the two machines.

[2] The slip power relationship for the BDFRM secondary winding has an exact analogy in the double-fed slip ring induction machine, where the slip recovery power is proportional to the slip.

[3] It can be seen in Appendix A that the pu values of these powers are $P_{pn} = (1/2)T_n$ and $P_{sn} = (\omega_{sn}/2)T_n$. These pu quantities emphasise that the secondary real power depends on the variable secondary frequency, whereas the primary real power is only determined by the output torque.

[4] In terms of slip, this can be expressed in a manner analogous to a conventional $2p_r$-pole induction machine i.e. $\omega_{rm} = (1 - s)\omega_p/p_r$.

slip as follows:

$$P_{s_{\text{rot}}} = \frac{s}{s-1} P_{\text{rot}} \tag{5}$$

The following observations can be made about (5) for a lossless machine. If $s = 0$ then the secondary power is zero, regardless of the output power. This corresponds to $\omega_s = 0$, which means that the BDFRM is operating as a $2p_r$-pole synchronous turbo machine (i.e. the secondary winding is supplying the DC field current). For $s = -1$ the secondary real power is one half the total shaft output power. In this case $\omega_s = \omega_p$, and both windings are carrying equal amounts of power. The other extreme condition is $s = 1$ when the machine is at standstill. It can be seen that the denominator of (5) is then zero, leading one to think that the secondary output power becomes infinity. However, this corresponds to a zero rotational output power condition, and therefore the power fed into the primary is regenerated back into the supply by the secondary. Needless to say this is the most inefficient machine mode that one can have since there is not output power, and the input power is feeding the losses of the machine. For all shaft speeds requiring a reversal of the phase sequence of the secondary (which means a negative ω_s), power is being supplied by the primary via expression (3) (note that this is only related to the output torque, and not the output power), whilst the secondary is returning power back to the supply so that the correct mechanical power is obtained.

To summarise the above discussion, one can see that the inverter connected to the secondary only has to be partially rated as far as the shaft rotational power is concerned. The specific rating of the inverter is related to how much the shaft speed varies from the "synchronous" speed of the machine i.e. it is determined by the generalised slip values s. For a full speed range, then the inverter should be rated at a maximum of half the output power. If the speed range required is restricted then the proportion of the output power supplied by the secondary is $s/(s-1)$.

An important influencing factor on the inverter size not mentioned in the previous discussion is the amount of imaginary power that the inverter has to handle (i.e. reactive power in steady state). Clearly the machine has to be magnetised in order to function, and the magnetisation current supplied via the inverter fed secondary winding (as compared to the non-inverter connected primary winding) will affect the rating of the inverter. The issues addressing this aspect are considered in detail in Section II-D.

B. Maximum Torque Per Total Amperes

From an efficiency viewpoint, another equally valid optimisation may be to maximise the generated torque for the *total amperes* into the machine – i.e. the sum of the primary and secondary winding current magnitudes. In order to make this analysis machine parameter independent the set of normalisations summarised in Appendix A have been used. After considerable manipulation one can get the following expression for the total input current in terms of the torque output, angles of the currents, and the inductance ratio $\zeta = L_p/L_{ps}$:

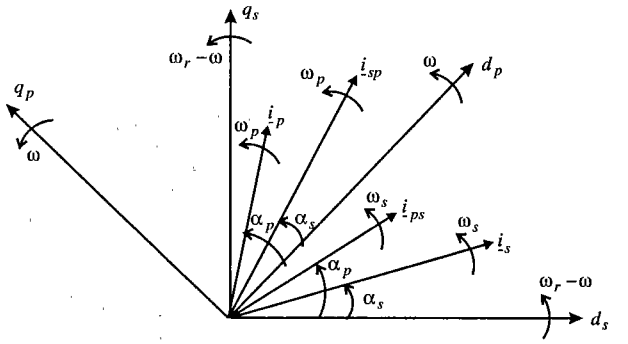

Fig. 2. Reference frames and current angles used for BDFRM modelling

$$i_{tn} = i_{pn} + i_{sn} = \frac{\zeta T_n}{2\sin\alpha_s} + \frac{2\tan\alpha_s - T_n}{2\tan\alpha_s \cos\alpha_p} \tag{6}$$

$$\tan\alpha_p = \frac{T_n \tan\alpha_s}{2\tan\alpha_s - T_n} \tag{7}$$

It should be noted that (7) automatically takes into account the constant flux and frame alignment conditions contained in (16).

Substituting for $\tan\alpha_p$ and rearranging we can obtain the total current expressed as a function of the secondary current angle and the torque:

$$i_{tn} = \frac{\zeta T_n \sqrt{1+\tan^2\alpha_s}}{2\tan\alpha_s} + \frac{\sqrt{(2\tan\alpha_s - T_n)^2 + T_n^2\tan^2\alpha_s}}{2\tan\alpha_s} \tag{8}$$

Fig. 3 presents a numerical solution of (8) for the optimal α_s that minimises i_{tn}. This could be stored in a look-up table for real-time control implementation on a DSP. The respective primary current angles α_p (Fig. 2) are calculated using (7). The plots throughout the paper have been generated assuming $\zeta = 9/7$, this corresponding to a typical SYNCREL saliency ratio of 8 [8]. One immediate observation from this figure is that α_s does not change as much with differing torque levels as α_p does. Note also that its value is only slightly greater than $\pi/4$, meaning that the secondary winding is participating in both the magnetisation of the machine and its torque production. The primary current, especially at lower torques, contributes mainly to the machine flux.

The plots of the individual current magnitudes for the windings (equation (15)) under the maximum-torque-per-total-amperes (MTPTA) angle conditions are presented in Fig. 4. It can be seen that the secondary current varies considerably with torque level as the latter is influenced primarily by the i_{sq}(see (1)), and α_s is higher than $\pi/4$ rads. Therefore as increased torque is required significant current change will occur in the

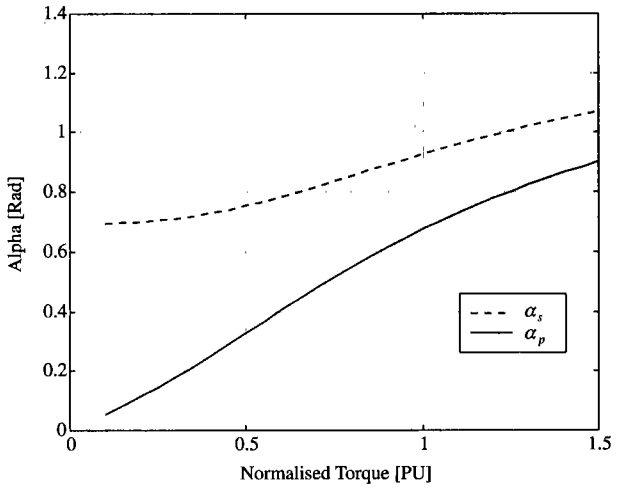

Fig. 3. α_s and α_p for maximum torque per $(i_{pn} + i_{sn})$

i_{sn} current due to a dominant q-axis component. The flux producing i_{pn} current, on the other hand, is almost constant as mentioned above.

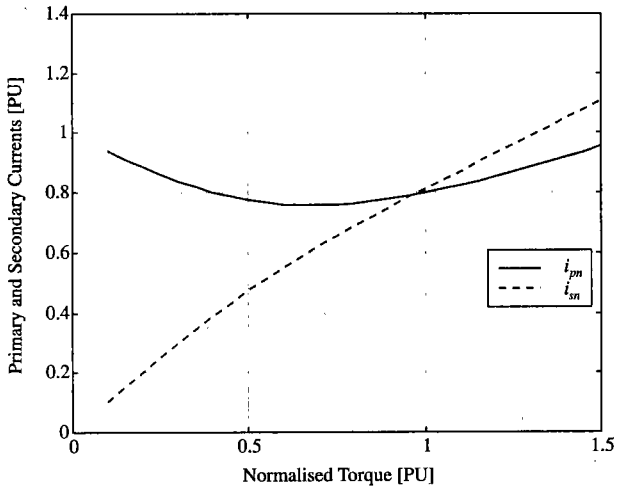

Fig. 4. Primary and secondary currents for MTPTA current angles

C. Constant Torque Operation

In order to investigate the effects of secondary current angle variations on the power flows in the BDFRM, (7) has been plotted for a variety of α_s with a constant torque $T_n = 1$. Fig. 5 shows the resulting locus of the current angles. These angles can be correlated with the power curves in Figs. 6 and 7 generated assuming the secondary applied frequency of $\omega_s = \omega_p$ i.e. $\omega_{sn} = 1$. One can see that $\alpha_p = \pi/2$ for unity primary power factor, which agrees with intuition. Also note that the primary and secondary windings carry equal amounts of real power as follows from (19) and (20). Therefore, in this case the inverter has to be rated to handle half the mechanical power produced by the machine, and the reactive power for the field.

If $\omega_{sn} < 1$ then it can be seen from (20) and (23) that both real and reactive power contributed by the secondary winding decrease proportionally with ω_{sn} and become zero at $\omega_{sn} = 0$ (for a lossless machine) when the BDFRM effectively behaves as a $2p_r$-pole synchronous machine with field control. For $\omega_{sn} < 0$ (this simply means the opposite phase sequence to the primary) the secondary winding functions as in slip energy recovery systems, with some of the real power from the primary winding being returned to the supply. One can easily conclude looking at (20) that a fractionally rated inverter is sufficient if the BDFRM is to be operated in a narrow range around the synchronous speed. This characteristic makes the BDFRM more than suitable for pump applications where the speed ratio is typically 2:1 or less.

Figs. 6 and 7 also demonstrate the primary winding power factor control capabilities of the BDFRM. However, this comes at a price – the secondary has to supply its own reactive power as well as that normally absorbed by the primary winding. The secondary power factor is consequently very bad in the low α_s region, and larger currents are required for the real power that is being supported by the secondary. This trend is clearly shown in Fig. 8 and will also be verified in the next section. A bidirectional converter feeding the secondary has to be rated appropriately if primary power factor control in these regions is desired. Note also that the minimum total current in Fig. 8 corresponds to the MTPTA α_s angle in Fig. 3 as expected. Furthermore, the total current is virtually constant at higher α_s angles (Fig. 8) as the d-axis secondary current is low since the machine flux is supplied by the primary, and the $\sin\alpha_s$ term in (1) means that i_s is virtually constant. As a result, the total current loading in this angle region is approximately equal to the primary current.

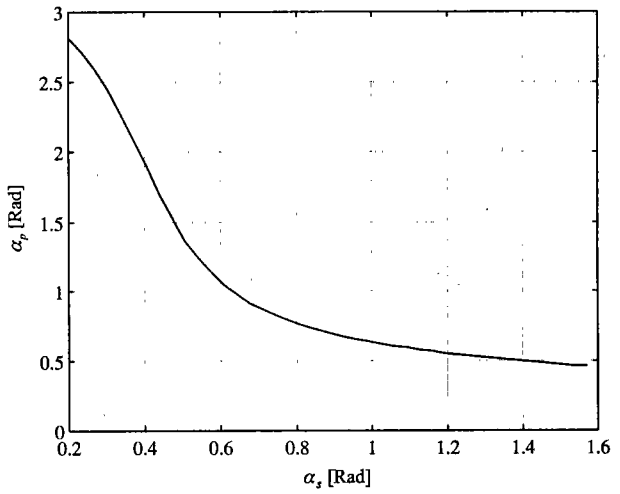

Fig. 5. The α_p and α_s angles for constant $T_n = 1$

D. Maximum Power Factor

One of the most important properties of the BDFRM is the inherently decoupled control of torque (primary power in generating mode) and primary reactive power

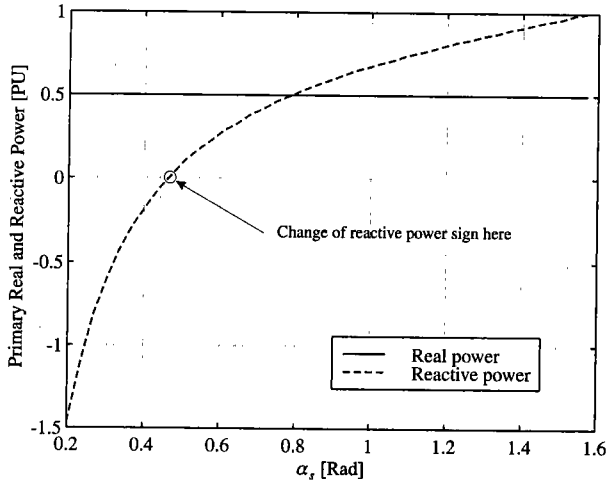

Fig. 6. Primary winding real (P_{pn}) and reactive (Q_{pn}) powers for $T_n = 1$

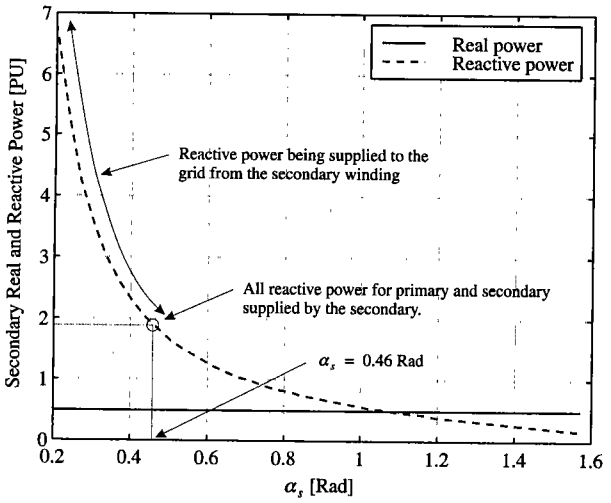

Fig. 7. Secondary winding real (P_{sn}) and reactive (Q_{sn}) powers under the $T_n = 1$ and $\omega_{sn} = 1$ condition

[5]. It is evident from (1) (or its normalised form (14)) and (22) that the secondary q-axis current is entirely responsible for torque production whereas the reactive power is only affected by the respective d-axis component. Therefore, even though the primary flux is fixed by the mains, we are still in a position to vary the grid power factor independently from torque. Unity primary power factor (UPPF) is obtained when $Q_{pn} = 0$ and occurs at:

$$\alpha_{s_{\text{uppf}}} = \tan^{-1} \frac{T_n}{2} \tag{9}$$

For $T_n = 1$ this is 0.46-rad as shown in Figs. 6 and 7.

From (7) the corresponding primary current angle is $\alpha_{p_{\text{uppf}}} = \pi/2$ at any torque (as noted previously). This result is expected as the primary current vector in quadrature with the flux producing d_p-axis contributes no flux in the machine. The secondary winding would be carrying all of the magnetising current in this case.

If the primary power factor performance is not an issue and the system cost is the major concern, then the

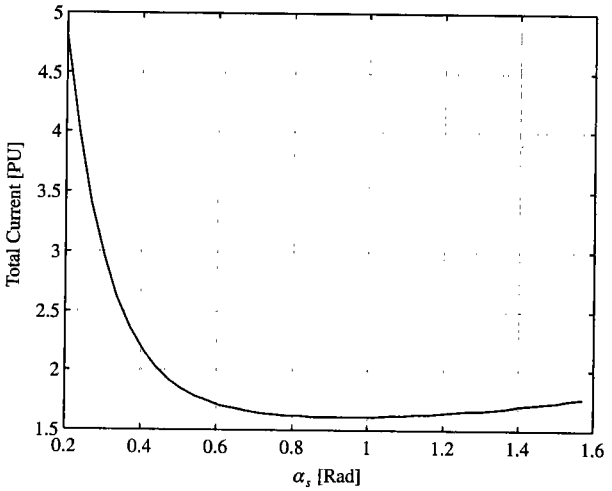

Fig. 8. Total current flowing into the machine at $T_n = 1$

minimum inverter VA rating i.e. the unity secondary power factor (USPF) is of interest. Setting $Q_{sn} = 0$ in (23), it can be obtained for USPF α_s:

$$\alpha_{s_{\text{uspf}}} = \tan^{-1} \frac{-\sqrt{1 - T_n^2(\frac{1}{k_{ps}^2} - 1)^2} - 1}{T_n(\frac{1}{k_{ps}^2} - 1)} > \frac{\pi}{2} \tag{10}$$

where k_{ps} is the coupling coefficient as defined in Appendix. Notice that although $Q_{sn} = 0$, $\alpha_{s_{\text{uspf}}}$ is not $\pi/2$ since the d_p-axis control frame chosen (Fig. 2) is along the primary (not secondary) flux vector. Another point to note is the significance of good magnetic interaction between the windings which is obvious from (23) – the higher k_{ps} the lower reactive power (Q_{sn}) and the better power factor ($\cos\phi_s$).

The plots of (9) and (10) for maximum power factor strategies that one would implement in a torque controller are presented in Fig. 9. The fact that the USPF secondary current has a demagnetising effect (as $\alpha_{s_{\text{uspf}}} > \pi/2$ i.e. $i_{sdn} < 0$) means that a significant extra d-axis current is needed in the primary to preserve constant flux in the machine. As a result, the USPF i_{pn} is about 2.5 its UPPF value (Fig. 10) the ratio being even higher at lower torques when most of the USPF i_{pn} current is flux producing (note the virtually flat curve in this torque range) and the UPPF current (a coupled i_{sqn} as $\alpha_{p_{\text{uppf}}} = \pi/2$ and $i_{pdn} = 0$) is small.

The other more important aspect of this power factor control is the influence it has on the inverter size required for a drive system. If the UPPF is desired, then the values of α_s are low and the secondary power factor is poor (Fig. 11) indicating an inefficient use of the inverter. Therefore, its current rating would have to be higher for a given output torque as anticipated earlier. This is illustrated by the top characteristic in Fig. 10, which also conforms with the results in Fig. 8.

The situation is diametrically opposite under the USPF conditions, as the α_s angles are above $\pi/2$ and the secondary carries less reactive current. One can see in Fig. 10 that $i_{sn_{\text{uspf}}} \approx 0.5 i_{sn_{\text{uppf}}}$ at $T_n = 1$ (and less at

lower torques) meaning that at least a half current rated inverter can be used in this case. However, the primary power factor is then a compromise and its maximum value is about 0.4 (Fig. 11).

If the machine is operated at the maximum torque per secondary ampere (MTPSA), the primary power factor can be somewhat improved and the inverter current rating further reduced but at the cost of moving away from the optimum inverter VA i.e. USPF point (Figs. 10 and 11). In regard to the primary power factor performance, the MTPTA strategy appears to be superior to the MTPSA as the power factor values vary from zero to approximately 0.79 (not shown in Fig. 11) over a torque range of 0 to 1.5-pu.

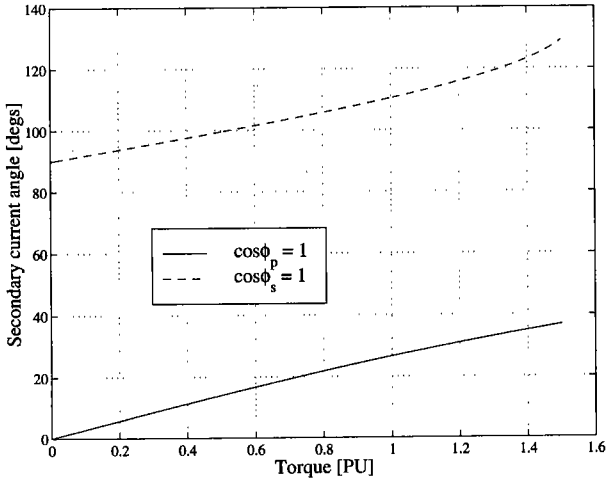

Fig. 9. Maximum power factor control angles at various torque levels

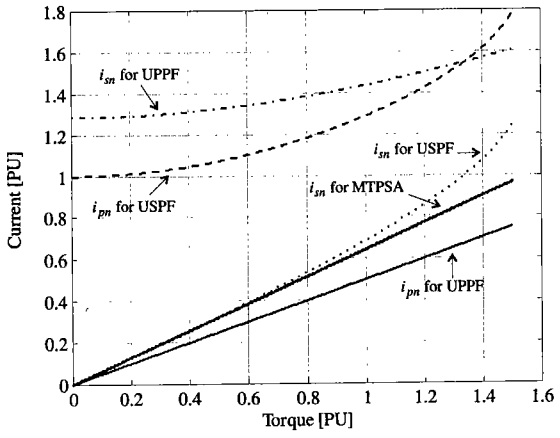

Fig. 10. Windings currents under the maximum power factor conditions

III. Conclusions

This paper has attempted to give an overall picture of the different optimal control strategies for the BDFRM and their inter-relationships. While the theoretical work presented is preliminary in nature, it has developed a number of useful control expressions that can serve as a basis for the machine's torque controller design. Another significant contribution of the paper is the investigation of various compromises between the machine performance and the inverter rating required.

It is clear from the analysis in this paper, and from other papers referenced, that for the same torque output the BDFRM has to be larger than an induction or synchronous machine. Therefore it is likely that the economics of machine/inverter size trade-offs will eventually decide the technological future and practical use of this interesting and unusual machine.

The development of a 6/2-pole axially-laminated prototype and a control system for implementation of the considered control methodologies is currently in progress. The results of this work will be presented in our future papers.

APPENDIX

I. Base Definitions and Values

The *normalisation bases* and *per unit expressions* for the BDFRM using standard notation are:

$$T_B = \frac{3}{4} p_r \frac{\lambda_p^2}{L_p} \qquad P_B = \frac{2\omega_B}{p_r} T_B \tag{11}$$

$$i_B = \frac{\lambda_B}{L_p} \qquad \lambda_B = \frac{v_B}{\omega_B} \qquad L_B = L_p \tag{12}$$

$$v_B; \omega_B \triangleq \text{the grid supply voltage;frequency} \tag{13}$$

$$T_n = \frac{2 \sin\alpha_s \sin\alpha_p}{\sin(\alpha_p + \alpha_s)} = \frac{2}{\zeta} i_{sn} \sin\alpha_s = \frac{2}{\zeta} i_{sqn} \tag{14}$$

$$i_{pn} = \frac{\sin\alpha_s}{\sin(\alpha_p + \alpha_s)}; \qquad i_{sn} = \frac{\zeta \sin\alpha_p}{\sin(\alpha_p + \alpha_s)} \tag{15}$$

$$\lambda_{pn} = \underline{i}_{pn} + \frac{1}{\zeta} \underline{i}_{sn}^* = 1 \tag{16}$$

$$= i_{pdn} + \frac{1}{\zeta} i_{sdn} + j \left(i_{pqn} - \frac{1}{\zeta} i_{sqn} \right) \tag{17}$$

$$\underline{\lambda}_{sn} = L_{sn} \underline{i}_{sn} + \frac{1}{\zeta} \underline{i}_{pn}^* \tag{18}$$

$$P_{pn} = \frac{1}{\zeta} i_{sn} i_{pn} \sin(\alpha_s + \alpha_p) = \frac{1}{2} T_n \tag{19}$$

$$P_{sn} = \frac{1}{\zeta} \omega_{sn} i_{sn} i_{pn} \sin(\alpha_s + \alpha_p) = \frac{\omega_{sn}}{2} T_n \tag{20}$$

$$P_n = P_{pn} + P_{sn} = \frac{1 + \omega_{sn}}{2} T_n = \omega_{rn} T_n \tag{21}$$

$$Q_{pn} = 1 - \frac{i_{sdn}}{\zeta} = \frac{\sin\alpha_s \cos\alpha_p}{\sin(\alpha_s + \alpha_p)} \tag{22}$$

$$Q_{sn} = \omega_{sn} \left[L_{sn} i_{sn}^2 + \frac{i_{sn} i_{pn} \cos(\alpha_s + \alpha_p)}{\zeta} \right]$$

$$= \frac{\omega_{sn} \sin\alpha_p}{\sin^2(\alpha_s + \alpha_p)} \left[\frac{\sin\alpha_p}{k_{ps}^2} + \sin\alpha_s \cos(\alpha_s + \alpha_p) \right] \tag{23}$$

where $\zeta = L_p / L_{ps}$ and $k_{ps} = L_{ps} / \sqrt{L_p L_s}$.

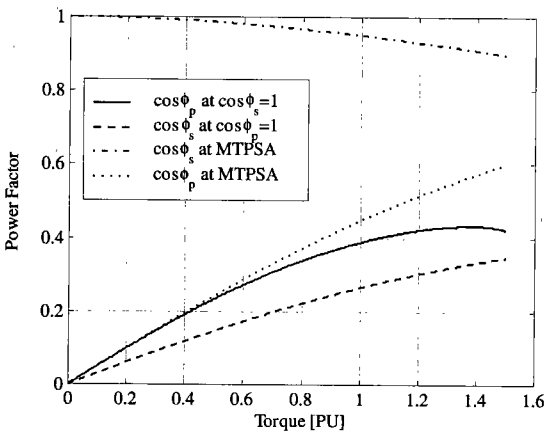

Fig. 11. Power factor performance for different control strategies

(Manuscript received Jan. 31, 2000, revised Sep. 18, 2000)

REFERENCES

[1] F. Liang, L. Xu, and T. Lipo, "D-q analysis of a variable speed doubly AC excited reluctance motor," *Electric Machines and Power Systems*, vol. 19, pp. 125–138, March 1991.

[2] L. Xu and Y. Tang, "A novel wind-power generating system using field orientation controlled doubly-excited brushless reluctance machine," *Proceeding of the IEEE IAS Annual Meeting*, pp. 408–418, 1992.

[3] Y. Liao, L. Zhen, and L. Xu, "Design of a doubly-fed reluctance motor for adjustable speed drives," *Proceedings of the IAS Annual Meeting*, vol. 1, pp. 305–312, Oct 1994.

[4] Y. Liao and C. Sun, "A novel position sensorless control scheme for doubly fed reluctance motor drives," *IEEE Trans Ind. Appl.*, vol. 30, pp. 1210–1218, Sept/Oct 1994.

[5] L. Xu, L. Zhen, and E. Kim, "Field-orientation control of a doubly excited brushless reluctance machine," *IEEE Transactions on Industry Applications*, vol. 34, pp. 148–155, January/February 1998.

[6] O. Ojo, "Field orientation control of a doubly-fed synchronous reluctance machine," *Proceedings of IEEE-PESC98*, vol. 2, pp. 1276–1282, June 1998.

[7] R. Betz and M. Jovanović, "Control aspects of brushless doubly fed reluctance machines," *Proceedings of the European Power Electroncis Conference (EPE'99)*, Sept. 1999.

[8] R. Betz and M. Jovanović, "The brushless doubly fed reluctance machine and the synchronous reluctance machine – a comparison," *Proceedings of the IEEE-IAS Annual Meeting*, Oct. 1999.

[9] F. Wang, F. Zhang, and L. Xu, "Parameter and performance comparison of doubly-fed brushless machine with cage and reluctance rotors," *Conference Record of the 2000 IEEE Industry Applications Conference*, Oct 2000.

[10] R. Betz and M. Jovanović, "Introduction to brushless doubly fed reluctance machines - the basic equations," Tech. Rep. EE0023, Department of Electrical Engineering, University of Newcastle, Australia, April 1998. Available at ftp://www.ee.newcastle.edu.au/pub/reb-/Papers/BDFRMRev.pdf.

[11] R. Betz and M. Jovanović, "Comparison of the brushless doubly fed reluctance machine and the synchronous reluctance machine," Tech. Rep. EE0024, Department of Electrical and Computer Engineering, University of Newcastle, Australia, October 1998. Available at ftp://www.ee.newcastle.edu.au-/pub/reb/Papers/bdfrm-sync.pdf.

[12] L. Xu and W. Cheng, "Torque and reactive power control of a doubly fed induction machine by position sensorless scheme," *IEEE Transactions on Industry Applications*, vol. 31, pp. 636–642, May/June 1995.

Milutin G. Jovanvić received the Dipl.Eng and M.E.E. degrees from University of Belgrade, Belgrade, Yugoslavia, in 1987 and 1991 respectively, and the Ph.D. degree from the University of Newcastle, Newcastle, Australia, in 1997. He is currently a Senior Lecturer in the School of Engineering, University of Northumbria, Newcastle upon Tyne, UK. His major interests lie in the areas of electrical machines and drives, power electronics and power systems. Dr. Jovanović is a member of the Industrial Drives Committee of the IEEE Industry Applications Society.

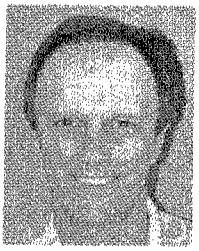

Robert E. Betz received the B.E., M.E. and Ph.D. Degrees from the University of Newcastle, Newcastle, Australia in 1979, 1982 and 1984 respectively. He is currently an Associate Professor in the Department of Electrical and Computer Engineering, University of Newcastle. His major interests are electrical machine drives, real-time operating systems, and industrial electronics. A/Professor Betz has been a Senior Research Fellow at the University of Glasgow, Scotland (1990-91), and the Danfoss Visiting Professor at Aalborg University, Denmark (1998). He is a member of the Industrial Drives Committee, and the Electric Machines Committee of the IEEE Industry Applications Society.